Biomaterials 32 (2011) 1068–1079

Contents lists available at ScienceDirect

Biomaterials

journal homepage: www.elsevier.com/locate/biomaterials

Chitosan/Poly(ε-caprolactone) blend scaffolds for cartilage repair

Sara C. Neves [a,b], Liliana S. Moreira Teixeira [c], Lorenzo Moroni [c], Rui L. Reis [a,b], Clemens A. Van Blitterswijk [c], Natália M. Alves [a,b], Marcel Karperien [c], João F. Mano [a,b,*]

[a] 3B's Research Group – Biomaterials, Biodegradables and Biomimetics, Headquarters of the European Institute of Excellence on Tissue Engineering and Regenerative Medicine, Department of Polymer Engineering, University of Minho, AvePark, Zona Industrial da Gandra, S. Cláudio do Barco 4806-909, Caldas das Taipas, Guimarães, Portugal
[b] IBB – Institute for Biotechnology and Bioengineering, PT Associated Laboratory, Guimarães, Portugal
[c] MIRA – Institute for BioMedical Technology and Technical Medicine, University of Twente, Department of Tissue Regeneration, P.O. Box 217, Enschede 7500 AE, The Netherlands

ARTICLE INFO

Article history:
Received 23 July 2010
Accepted 19 September 2010
Available online 27 October 2010

Keywords:
Chitosan
Polycaprolactone
Scaffold
Cartilage tissue engineering

ABSTRACT

Chitosan (CHT)/poly(ε-caprolactone) (PCL) blend 3D fiber-mesh scaffolds were studied as possible support structures for articular cartilage tissue (ACT) repair. Micro-fibers were obtained by wet-spinning of three different polymeric solutions: 100:0 (100CHT), 75:25 (75CHT) and 50:50 (50CHT) wt.% CHT/PCL, using a common solvent solution of 100 vol.% of formic acid. Scanning electron microscopy (SEM) analysis showed a homogeneous surface distribution of PCL. PCL was well dispersed throughout the CHT phase as analyzed by differential scanning calorimetry and Fourier transform infrared spectroscopy. The fibers were folded into cylindrical moulds and underwent a thermal treatment to obtain the scaffolds. μCT analysis revealed an adequate porosity, pore size and interconnectivity for tissue engineering applications. The PCL component led to a higher fiber surface roughness, decreased the scaffolds swelling ratio and increased their compressive mechanical properties. Biological assays were performed after culturing bovine articular chondrocytes up to 21 days. SEM analysis, live-dead and metabolic activity assays showed that cells attached, proliferated, and were metabolically active over all scaffolds formulations. Cartilaginous extracellular matrix (ECM) formation was observed in all formulations. The 75CHT scaffolds supported the most neo-cartilage formation, as demonstrated by an increase in glycosaminoglycan production. In contrast to 100CHT scaffolds, ECM was homogenously deposited on the 75CHT and 50CHT scaffolds. Although mechanical properties of the 50CHT scaffold were better, the 75CHT scaffold facilitated better neo-cartilage formation.

1. Introduction

Articular cartilage (AC) regeneration using tissue engineering (TE) approaches has been primarily proposed due to its limited capacity of self-repair [1,2]. This mainly derives from the lack of a vasculature network, resulting in insufficient turn-over of healthy chondrocytes to the defective sites and low productivity of characteristic proteins of the surrounding extracellular matrix (ECM) [1,2]. Three-dimensional (3D) scaffolds are particularly important for AC TE approaches because the chondrogenic phenotype is maintained when chondrocytes are placed in a proper 3D environment [2].

Cartilage-specific ECM components play an important role in regulating expression of the chondrogenic phenotype and supporting chondrogenesis [3,4]. Chitosan (CHT), a naturally derived polysaccharide, is an excellent candidate as AC TE scaffolding biomaterial, due to its structural similarity with various glycosaminoglycans (GAGs) found in cartilage [5]. It was shown to support chondrogenic activity [5] and to allow cartilage ECM proteins expression by chondrocytes [6,7]. However, the brittleness in the wet state (40–50% of strain at break) of CHT scaffolds [8] is a major drawback for application in AC TE.

Among synthetic biomaterials, poly(ε-caprolactone) (PCL) is highly appealing due to its (a) physical-chemical and mechanical characteristics [9], (b) easy process ability related to a relatively low melting temperature (ca. 60 °C) [8], (c) non-toxic degradation products and (d) Food and Drug Administration (FDA) approval for biomedical applications [9]. It has been previously reported that chondrocytes attach and proliferate on PCL films [10] and, additionally, start to produce a cartilaginous ECM in PCL scaffolds [11,12]. However, PCL main drawbacks as scaffolding material

* Corresponding author. 3B's Research Group – Biomaterials, Biodegradables and Biomimetics, Headquarters of the European Institute of Excellence on Tissue Engineering and Regenerative Medicine, Department of Polymer Engineering, University of Minho, AvePark, Zona Industrial da Gandra, S. Cláudio do Barco 4806-909, Caldas das Taipas, Guimarães, Portugal. Tel.: +351 253510904; fax: +351 253510909.
E-mail address: jmano@dep.uminho.pt (J.F. Mano).

0142-9612/$ – see front matter © 2010 Elsevier Ltd. All rights reserved.
doi:10.1016/j.biomaterials.2010.09.073

comprise the (a) absence of cell recognition sites, (b) its hydrophobicity and (c) its relatively slower degradation/resorption kinetics compared to other polyesters [13,14].

When combined, the hydrophilic nature of CHT will enhance the wettability and permeability, with a consequent acceleration of PCL hydrolytic degradation. The PCL component is expected to lower the swelling ratio and improve the wet state mechanical properties of CHT scaffolds [15]. Moreover, the bioactivity of PCL can be enhanced when combined with natural polymers [16], as submicron phase separation of hydrophilic and hydrophobic domains could be beneficial for cell adhesion.

Different methodologies have been used to combine CHT and PCL. Due to its simplicity and effectiveness, blending allows tailoring the materials properties by adjusting the blend composition [17]. Moreover, polymers can co-exist with minimal chemical modification [8]. However, common solvents for CHT and PCL are scarce. 1,1,1,3,3,3-hexa-fluoro-2-propanol (HFIP) [18,19] or acetic acid [8,20] are, by far, the most used solvents. However, HFIP is very toxic, carcinogenic, expensive and difficult to remove [21]. Alternatively, diluted acetic acid solutions lead to phase separation [20].

3D scaffolds of blends of CHT and PCL for TE applications have been previously developed by freeze-drying [22] and particle-leaching [23,24]. 3D fiber-mesh scaffolds started to be used in TE applications [25,26] as they present (a) an increased surface area for cell attachment [2], (b) improved pore architecture [2], and (c) good mechanical stability [2]. Processing CHT/PCL blends fibers was reported for the first time by electros pinning, first for neural TE applications [27], and later in bone TE applications [28]. Recently, Malheiro et al. [17] processed non-woven fibers of blends of CHT and PCL, by wet-spinning. A common solvent solution of 70:30 vol.% formic acid/acetone was used and preliminary studies were performed on folding the fibers to obtain 3D fiber-meshes. Shalumon et al. [29] processed CHT/PCL blend electrospun fibers using this solvent solution.

The aim of the present work was to develop CHT/PCL blend scaffolds, based on a previous methodology to produce CHT/PCL fibers [17]. Furthermore, the suitability of these structures as cartilage TE supports was analyzed. Three different formulations – 100:0, 75:25 and 50:50 wt.% CHT/PCL – were used, in order to investigate the effect of polymer composition in the physical-chemical and biological properties of the fiber-meshes.

2. Materials and methods

2.1. Materials

CHT (low molecular weight, 75–85% deacetylation degree, Ref. 448869), PCL (80 KDa, Ref. 440744), formic acid, and methanol were purchased from Sigma–Aldrich. The solvents were used without further purification. CHT was purified by recrystallization before being used, as described elsewhere [17]. Briefly, it was dissolved in 1% (wt./vol.) acetic acid solution and then filtered through porous membranes (Whatman® ashes filter paper, 20–25 μm, and nylon filter sheet) into a Buckner flask under vacuum. Adjusting the pH of the solution to about 8, through the addition of NaOH, caused flocculation due to deprotonation and insolubility of the polymer at neutral pH. The polymer was then neutralized until the pH equaled that of distilled water, frozen at −80 °C and lyophilized. Polymeric solutions with distinct concentrations were prepared according to the concentrations presented in Table 1.

Table 1
Total polymer concentration of each fiber composition [47].

Formulation	CHT/PCL weight ratio	Total Polymer Concentration (wt./vol. %)
100CHT	100:0	13
75CHT	75:25	17
50CHT	50:50	21

2.2. Methods

2.2.1. Scaffold preparation

The polymeric solutions of CHT and CHT/PCL blends were prepared by dissolving CHT and PCL in 100 vol.% formic acid, in the proportions of 100, 75, and 50 wt.% in CHT content (Table 1), from now referred to as 100CHT, 75CHT, and 50CHT, respectively. The solutions were left at 30 °C overnight for a complete dissolution of both polymers. After that, the solutions were placed into a 5 mL syringe with a capillary tip having an inner diameter of 0.8 mm. A syringe pump was used to feed the solutions into the needle tip. A coagulation bath of methanol was used to precipitate the solutions (0.1 mL to obtain a continuous fiber, in order to process one scaffold), and no air gap was left between the tip and the referred bath during the extrusion. The fibers were left in the methanol bath overnight to complete the solidification process. They were neutralized with 1M NaOH solution to fully regenerate the free amine form of the polymer chains and to avoid any CHT re-dissolution. Afterwards, the fibers were washed (at least four times) with distilled water until the pH reached a physiological value. Subsequently, they were dehydrated in a series of ethanol aqueous solutions (50, 70, 90 and 99.9 vol.% ethanol), folded in plastic cylindrical moulds and dried in an oven at different temperatures (T_a = 45, 50, 55, 60, 65 and 75 °C) for either t_a = 1.5 h or 3 h, in a similar way as described in [17].

2.2.2. Characterization

2.2.2.1. Scanning electron microscopy (SEM). An XL 30 ESEM-FEG Philips microscope was used to analyze the phase structures of the fibers, before and after solvent etching, to evaluate the over all 3D structure of the constructs and for chondrocyte proliferation and differentiation studies. Prior SEM analysis, the constructs were fixed with formalin (only for the biological assays), dehydrated using graded ethanol solutions and critical point dried (Balzers CPD 030). All samples were coated with gold (Cressington Sputter Coater). The analysis was performed at an accelerating voltage of 10 kV and magnifications from 200× to 2000×.

2.2.2.2. Differential scanning calorimetry (DSC). The DSC experiments were conducted in a Q100 calorimeter with refrigerated cooling system (TA Instruments). Prior the scans, the temperature and energy calibrations were performed with an indium standard. All the samples were (a) left at 0 °C for 2 min, (b) heated from 0 to 100 °C, (c) left at 100 °C for 2 min to erase the thermal history, (d) cooled down to 0 °C, (e) left again at 0 °C for 2 min, and (f) re-heated to 100 °C. The heating and cooling rate was of 10 °C/min. The melting temperature (T_m) and melting enthalpy (ΔH_m) of PCL were determined from the first and second heating scans. The peak temperature (T_m) and peak area (ΔH_m) values were calculated using the TA Instruments Universal Analysis software. The crystallinity degree (χ_c) can be calculated applying equation (1).

$$\chi_c = \Delta Hm/\Delta H_u^0 w \quad (1)$$

where $\Delta H_u^0 w$ is the melting enthalpy of 100% crystalline PCL (i.e. 166 J/g [17]) and w is the weight fraction of PCL in the blend.

2.2.2.3. Fourier transform infrared (FTIR) Spectroscopic imaging measurements. A Perkin–Elmer Spectrum Spotlight 200 FTIR Microscope System was used to perform the imaging measurements. The sample fibers were embedded in a resin (Epofix Kit, Struers, composition as given by the company: bisphenol-A-(epichlorhydrin), epoxy resin, oxirane and mono[(C12-14-alkyloxy)methyl] resin) for further cross-sections observation and consequent analysis in order to study the distribution of the polymers in the fibers. The preparation of the raw PCL sample consisted in a transversal cut of a PCL bead. The resin was left to solidify overnight at room temperature and the samples were subsequently cut into ≈10 μm thick slices. The sectioning of the resin embedded samples was performed with a Leitz 1401 microtome using a glass knife at room temperature. Spectra were collected in continuous scan mode in order to construct FTIR maps, with an area of 240 × 240 μm^2 and a spectral resolution of 16 cm^{-1}, by averaging 15 scans for each spectrum. The samples were analyzed in transmittance. Both spectra were collected in the spectral range of 4000–720 cm^{-1} and integrated by taking the areas under the curve between the limits of the peaks of interest. The chosen region for CHT identification corresponds to C=O stretching of amide I, centered at approximately 1650 cm^{-1} [30], and for the PCL the carbonyl stretching absorption at about 1730 cm^{-1} [30]. There is also a characteristic peak of CHT that corresponds to the amine deformation vibration, centered at 1590 cm^{-1}, but it could not be used due to overlap with an epoxy resin characteristic peak. To represent PCL and CHT in the chemical maps, the carbonyl stretching band was integrated between 1760 and 1710 cm^{-1}, while for CHT the integrated intensity of the band from 1670 to 1630 cm^{-1} was evaluated.

2.2.2.4. Micro-computed tomography (μCT). The fiber-mesh scaffolds were analyzed using a high-resolution micro-computed tomography (μCT) Skyscan 1072 scanner (Skyscan, Kontich, Belgium). The scaffolds were scanned in a high-resolution mode using a pixel size of 8.70 μm and integration time of 1.7 ms. The X-ray source was set at 50 keV of energy and 201 μA of current. Representative data sets of 150 slices were transformed into a binary picture using a dynamic threshold of 60–255 (grey values) to distinguish polymer material from pore voids. This data was used for

morphometric analysis (CT Analyser v1.5.1.5, SkyScan), which included quantifying the porosity and pore size. 3D virtual models of representative regions in the bulk of the scaffolds were also created, visualized, and registered using both image processing softwares (ANT 3-D creator v2.4, SkyScan).

2.2.2.5. Swelling tests. For the swelling studies, dried scaffolds of each formulation were weighted (W_d) – prior immersion in phosphate-buffered saline (PBS) for 24 h, at 37 °C. After 2, 4, 6, 8 and 24 h of immersion, the samples were weighted (wet, W_s) ($n = 2$). The superficial water was removed prior weighing with oil paper. The swelling ratio (Q) was obtained using equation (2).

$$Q = (W_s - W_d)/W_d \quad (2)$$

2.2.2.6. Mechanical properties. The mechanical behavior of the three formulation scaffolds in wet state was tested, under static compression solicitation. The scaffolds were immersed in phosphate-buffered solution (PBS) at physiological pH (≈7.4) and temperature (≈37 °C) for 3 days for complete hydration. The unconfined static compressive mechanical properties of the scaffolds were measured using an INSTRON 5543 (Instron Int. Ltd., U.S.A.), with a load cell of 1 kN, for 60% of strain, at a loading rate of 2 mm/min. The initial linear modulus on the stress/strain curves ($n = 3$), obtained by the secant method, defines the compressive modulus (or Young modulus).

2.2.2.7. Chondrocyte Isolation and seeding. Bovine cartilage was harvested from the patellar–femoral groove of calf legs. Cartilage tissue was cut into small pieces and chondrocytes were isolated by incubation in Dulbecco's modified Eagle's medium (Gibco) (DMEM) containing 0.2% type II collagenase at 37 °C for 8 h. The isolated chondrocytes were washed, centrifuged and re-suspended in DMEM with 10% heat inactivated fetal bovine serum (FBS, Sigma–Aldrich), Penicillin/Streptomycin 100U/100 μg/mL (Invitrogen), 0.1 mM MEMnonessential amino acids (Gibco), 0.2 mM ascorbic acid 2-phosphate (Invitrogen) and 0.4 mM proline (Sigma–Aldrich) and culture expanded. At confluence, the cells were detached using 0.25 wt.% trypsin in sterile PBS, washed with PBS, re-suspended in culture medium, and seeded (passage 2) on the scaffolds. The seeded constructs were incubated with the medium referred above.

For chondrogenic activity assessment studies, freshly isolated chondrocytes (passage 0) from the cartilage tissue were immediately seeded on the scaffolds and the constructs were cultured in chondrocyte differentiation medium composed of high glucose DMEM with 0.1 μM dexamethasone (Sigma), 2 mM L-glutamine (Glutamax, Gibco), 100 μg/mL sodium pyruvate (Sigma), 0.2 mM ascorbic acid 2-phosphate (Invitrogen), 0.4 mM proline (Sigma–Aldrich), 50 mg/mL insulin–transferrin–selenite (ITS + Premix, BD biosciences), 100 μg/mL penicillin, 100 μg/mL streptomycin and 10 ng/mL transforming growth factor-β3 (TGF-β3, R&D Systems).

Prior cell seeding in both studies, the scaffolds were sterilized by immersion in a solution of 70 vol.% of ethanol for 4 h, washed in PBS for 1 h (three times) and left immersed in PBS overnight. Then, the scaffolds were incubated in the following culture media for 2 days: proliferation medium for cell viability studies and differentiation medium (serum-free) for chondrogenic activity studies. Cells in culture flasks and on scaffolds were incubated in a humidified atmosphere of 5% CO_2 at 37 °C. The medium was replaced every 2 or 3 days. For both proliferation and differentiation studies, each scaffold was seeded with 5×10^5 cells (in 20 μL of cell suspension).

2.2.2.8. Cell viability studies. Cell viability and metabolic activity was studied using a Live-dead assay and MTT [3-(4,5-dimethyl-2-thiazolyl)-2,5-diphenyl-2HO tetrazolium bromide] assay. At days 1, 3, 7, 14 and 21, the 3D constructs were rinsed with sterile PBS and stained with calcein/ethidium homodimer using the Live-dead assay Kit (Invitrogen). Sections were immediately examined with an inverted fluorescence microscope (Nikon Eclipse E400) using a FITC/Texas Red filter. Calcein AM is capable of permeating the plasma membrane of viable cells, where it is cleaved by intracellular esterases - and produces green fluorescence. Ethidium-bromide homodimer-1 is able to enter cells with damaged membranes and binds to fragmented nucleic acids, thereby producing red fluorescence in dead cells.

MTT staining was performed using 1% (total medium volume) of MTT solution (5 mg/mL, Gibco) and an incubation time of 2h. Samples were visualized using a light microscope. Dissolved MTT can be converted to an insoluble purple formazan by dehydrogenase enzymes that catalyze the cleavage of the tetrazolium ring in MTT.

2.2.2.9. Chondrogenic activity and extracellular matrix production assessment studies. For histological analysis, samples were fixed in 10% formalin for 1 h, embedded in paraffin, and processed using standard histological procedures. Sections (5 μm thick) were obtained with a microtome and used for all stainings. After rehydration with xylene and an ethanol series (from 100 to 70 vol.%) the samples were stained with safranin-O/fast green [31] and alcian blue/nuclear fast red [32]. Slides were assembled with resinous medium for visualization using a light microscope (Nikon Eclipse E400) and representative images captured using a digital camera (Sony Corporation, Japan) and Matrix Vision Software (Matrix Vision GmbH, Germany).

DNA and GAG quantification assays were performed after 1, 14, and 21 days of culture in differentiation medium. The constructs were taken from the chondrocyte differentiation medium, washed in PBS and frozen at −80 °C until further processing. Afterwards, they were digested overnight at 56 °C (>16 h) in a Tris-EDTA buffered solution containing 1 mg/mL proteinase-K, 18.5 μg/mL pepstatin A, and 1 μg/mL iodoacetamide (Sigma–Aldrich).

Quantification of total DNA was performed with Cyquant dye kit according to the manufacturers description (Molecular Probes, Eugene, Oregon, U.S.A.), using a spectrofluorometer (Victor^3, Perkin–Elmer, U.S.A.), at an excitation wavelength of 480 nm and an emission wavelength of 520 nm ($n = 3$, in triplicate).

GAG amount was determined spectrophotometrically (Monochromator Microplate Reader TECAN Safire2, Austria) after reaction with dimethylmethylene blue dye (DMMB, Sigma–Aldrich) by measuring absorbance at 520 nm. The final amount was calculated using a standard of chondroitin sulphate B (Sigma–Aldrich) ($n = 3$, in triplicate).

2.2.2.10. Statistical analysis. Values on this study are reported as mean and standard deviation. Statistical analysis was performed using the one-way ANOVA test, with $p < 0.05$ considered as being statistically significant.

3. Results and discussion

3.1. Physical-chemical characterization of cht/pcl fibers

100CHT, 75CHT and 50CHT fibers were successfully obtained. The approach reported by Malheiro et al. [17] was modified into a simpler system, where the solvent solution is composed of 100 vol.% of formic acid.

Phase morphology and surface properties are important parameters to be considered when a scaffold is being designed. The homogeneity of the CHT/PCL polymeric blends is not only important in terms of their internal structural and mechanical integrity, but also in terms of PCL superficial domains distribution. Therefore, solvent etching was performed and the fiber surfaces were analyzed by SEM (Fig. 1), before and after etching. In order to remove the PCL phase of the blends, sample fibers were immersed in chloroform for 24 h, which dissolves PCL but not CHT. Before etching, fiber's topography (Fig. 1 (a–c)) varied between the three formulations with an increase in surface roughness with increasing PCL concentration. After etching (Fig. 1 (d–f)), the blends kept their dimensional stability, indicating that the CHT is the continuous phase in the blend. This is consistent with Cruz et al. [20], who reported the presence of a continuous CHT phase starting at 20 wt.% CHT content. Pore formation was also observed on the fiber surface after etching, thus confirming PCL extracted domains, with sizes in the micron scale. The distribution of the pores was rather homogeneous in both blends. As expected, lower pore formation was observed in etched 75CHT fibers, when compared to 50CHT fibers. Such distribution of more hydrophobic (PCL) regions dispersed in a more hydrophilic phase (CHT) may promote protein adsorption and cell attachment under physiological conditions.

The miscibility of the blend components was analyzed by evaluating the changes in the T_m as a function of composition using DSC. The DSC analysis was focused on the thermal properties of the PCL phase in the blends. Thus, the temperature range chosen was from 0 °C to 100 °C to cover the melting and crystallization processes of the PCL component. The trends obtained (from the first and second heat scans) are presented in Fig. 2(a, b). Two heating scans were carried out, being the first one used to infer about any effect of processing on the development of the PCL structure. Analyzing the graphs presented on Fig. 2 (c, d), both the T_m and χ_c values of PCL in the blends did not vary significantly from the values of pure PCL.

The information given by the DSC analysis about polymer mixing homogeneity could offer a preliminary insight about the interaction of both polymer phases in the blends. CHT and PCL are thermodynamically not miscible, and although they may present some compatibility degree, this mainly depends on the preparation method [30]. As already pointed out by Olabarrieta et al. [33], a high

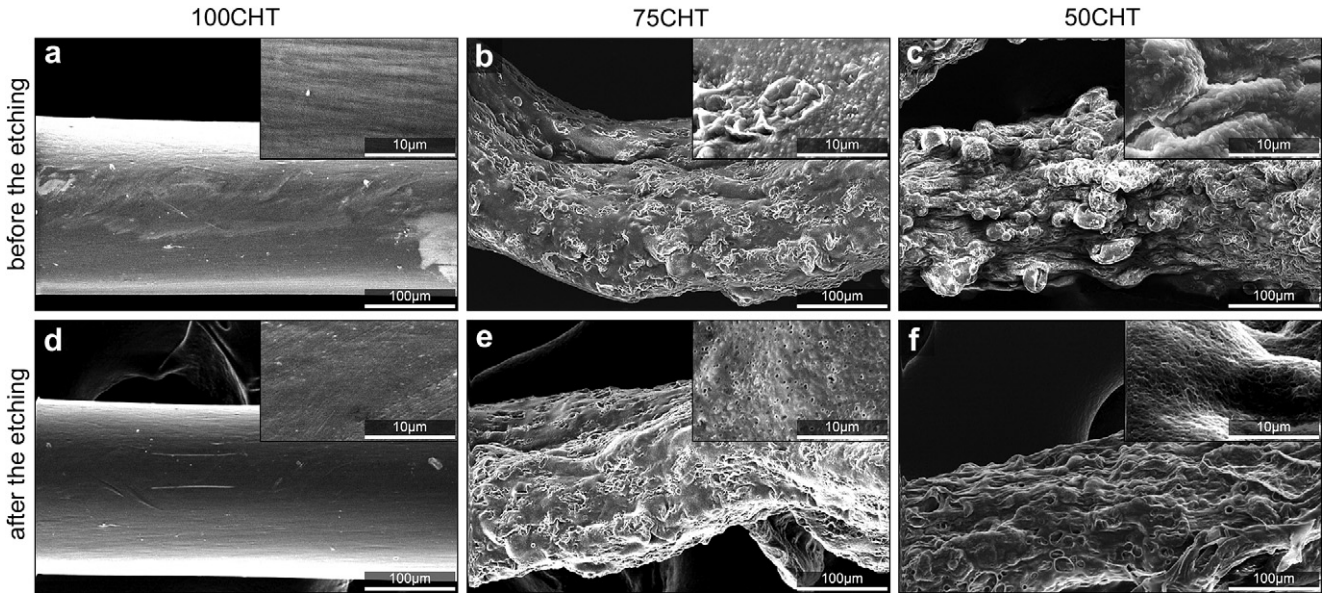

Fig. 1. SEM microphotographs of the fibers surfaces, (a, b, c) before and (d, e, f) after the solvent etching procedure.

degree of dispersion occurs between PCL and CHT phases, although mixing is not observed at a molecular level [33]. Some authors pointed out that the melting depression of PCL in CHT/PCL blends (using HFIP [19] and aqueous acetic acid solution as solvents [8,34]) is an indication of the miscibility of PCL and CHT. Here, we did not find any linear relationship between the CHT content and the T_m variation, as it did not vary significantly, when compared to pure PCL. This may indicate that phase separation exists between the

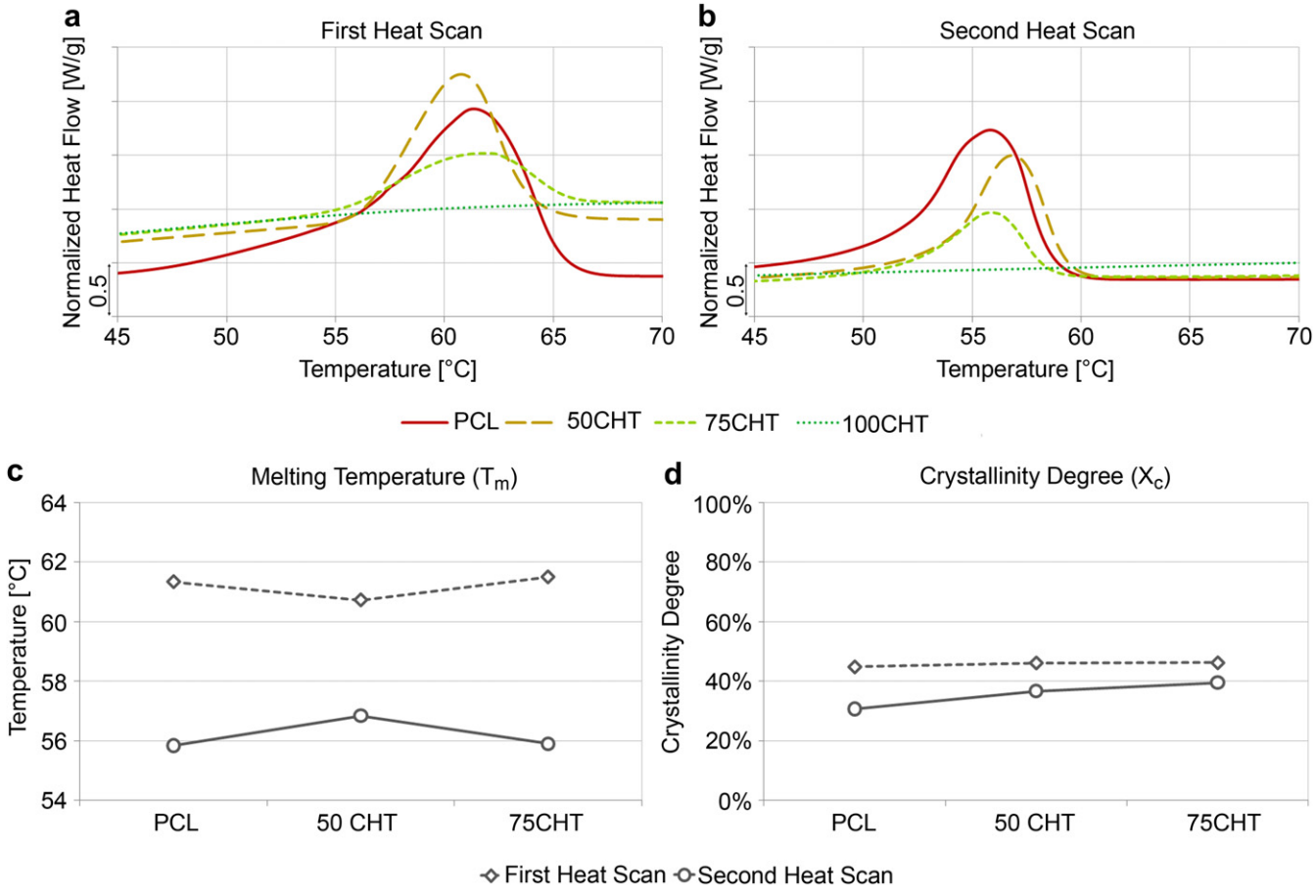

Fig. 2. DSC (a) first and (b) second heating scans for PCL, CHT and their blend fibers; PCL and blend fibers (c) melting temperature (T_m) and (d) crystallinity degree (χ_c) variations.

two polymers. The PCL domains may aggregate and crystallize without significant interference from CHT. Such assumption is supported by the SEM images (Fig. 1 (d–f)) that show the superficial features of the removed PCL domains. Corroborating this assumption, no significant variations on the χ_c of the blend fibers were observed when compared to pure PCL (Fig. 2 (d)).

FTIR analysis was performed in 10 μm thick sections of fibers embedded in epoxy resin to evaluate the distribution of CHT and PCL in the fiber's cross-sections. FTIR spectra and associated chemical maps are presented in Figs. 3 and 4, respectively. Fig. 3 (a) shows the spectra of the individual components, PCL and CHT, and epoxy resin. There is a variety of detectable absorption bands specific for PCL and CHT. The most obvious distinguishing features are a C=O stretching of amide I centered at 1650 cm^{-1} and an amine deformation vibration centered at 1590 cm^{-1}, which is specific for CHT, and a carbonyl stretching absorption at 1730 cm^{-1} for PCL. Fig. 3 (b) shows the spectra of the blends. These show that no significant frequency shifts of the characteristic functional groups occurred, when compared to pure polymers spectra. This may also indicate that no molecular interactions happened between the referred groups, corroborating previous works conclusions about the interaction between the two polymers in blends [17,35].

The blends chemical mapping (Fig. 4 (c, d)) showed a predominant yellowish color and the individual polymeric maps similar intensities across the sectioned areas. Thus, although the polymers are not miscible, the PCL domains over CHT seem to be well dispersed at the intrinsic length scale of the technique used, having sizes with dimensions lower than 10 μm.

The used method permitted to disperse PCL domains throughout CHT phase at the micron-level. Thus, homogeneous wet-spun blend fibers were obtained and, as only one common non-aqueous solvent system was used, PCL precipitation during the polymeric solutions preparation was avoided.

3.2. 3D fiber-mesh scaffolds characterization

To increase fiber adhesion after molding, the scaffolds were thermally treated. In this study, the fibers were heated at a temperature (T_a) near the T_m of PCL during different periods of time (t_a). Fibers connectivity of each formulation was analyzed by SEM for each combination of temperature and time (data not shown). The optimal condition was $T_a = 60$ °C and $t_a = 3$ h. The obtained fiber connectivity can be observed in Fig. 5 (a–c), with respective magnifications in Fig. 5 (d–f). In this condition the fibers were connected and maintained the 3D mesh pore network. At $T_a < 60$ °C fibers could be easily unfolded and no physical connection was observed in SEM analysis. At $T_a > 60$ °C the superficial PCL melted and was spread over the fiber surface. Fiber adhesion almost exclusively depended on the pre-melting or melting of superficial PCL, which resulted in satisfactory fiber-mesh stability as the constructs could be easily handled and kept their shape even in a swollen state.

μCT analysis performed resulted in an indicative calculated porosity and pore size (Table 2) from the selected volume of which the reconstructed 3D images are presented on Fig. 5 (g–i). The analysis also revealed an adequate scaffold porosity range for TE applications and a pore size in the acceptable range from 250 μm to

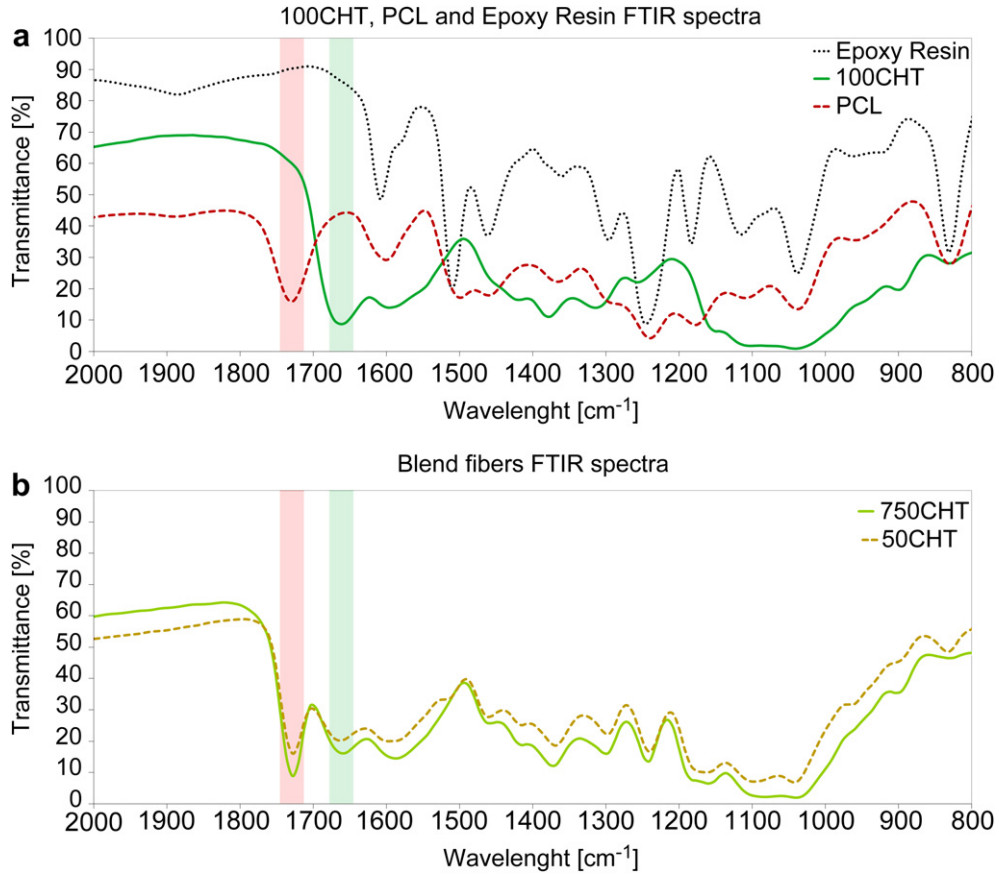

Fig. 3. Conventional FTIR spectra (only the 2000–800 cm^{-1} range is shown) of (a) 100CHT (solid line), PCL (dashed line) and epoxy resin (dotted line) and (b) of the blend fibers (solid line for 75CHT and dashed line for 50CHT). The shadow bands identify the regions that have been selected for the integration procedure used to obtain the images on Fig. 4.

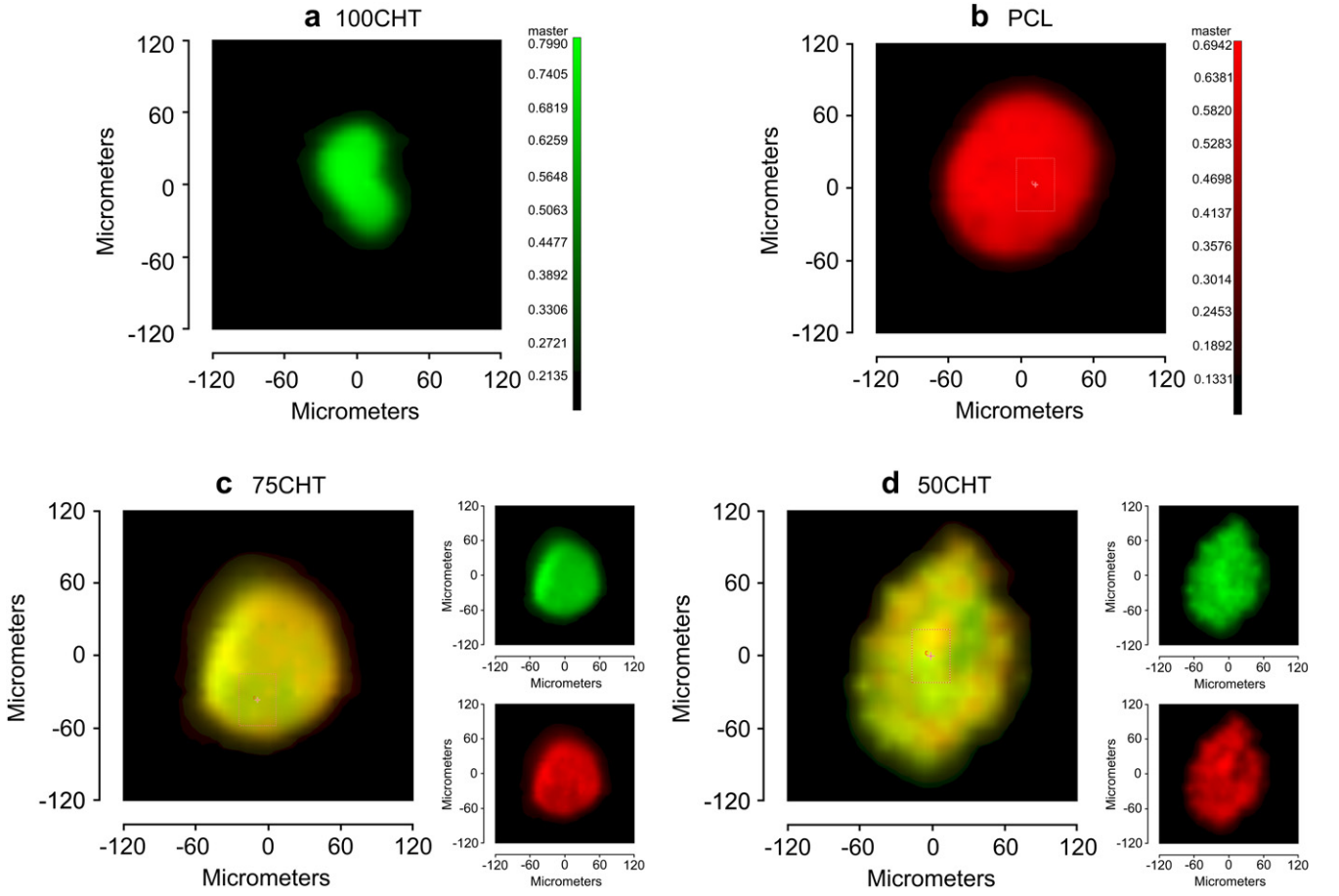

Fig. 4. Chemical maps of four discrete compositions of the fibers cross-sections. The different color intensities that can appear in the images may result from the cross-sections different thicknesses. Green indicates the presence of CHT, red the presence of PCL and black corresponds to the epoxy resin. The smaller images present on the right side of the blends chemical maps individualize the presence of the CHT and the PCL in the blends.

500 μm as suggested by Lien et al. [31] to support chondrogenic activity and consequent ECM production. The 3D reconstruction showed similar internal structure between scaffold formulations and highly interconnected pores. However, as the μCT was performed to scaffolds in dry state, it should be mentioned that the scaffold's behavior in a physiological environment would likely result in a different pore size due to swelling and water uptake.

The swelling behavior of the 3D fiber-meshes (Supplementary Fig. S1 (a)) is an important parameter to be evaluated. The physiological conditions imply a hydrated state of the fibers, also providing an insight about the water affinity degree that the scaffolds may have, when comparing formulations. The 100CHT scaffolds showed the highest swelling ratio, followed by the 75CHT and by the 50CHT composition. The increase in PCL (hydrophobic) content in the blends decreased the swelling when compared to 100CHT scaffolds. This reinforces the hypothesis that PCL improves CHT mechanical properties, as the poor mechanical properties of CHT (when compared to the blends) mainly derives from its swollen wet state.

Compression tests were performed to evaluate the mechanical performance of the 3D fiber-meshes in a wet environment, mimicking the physiological conditions. The results for the Young modulus are presented in Table 2 and a representative curve for the deformation behavior of each of the three different fiber-mesh scaffolds is presented on the graph of Supplementary Fig. S1 (b). The formulation with lowest Young modulus value corresponds to 100CHT, followed by 75CHT and 50CHT. Therefore, as the quantity of PCL increases, the scaffolds Young modulus also increases.

3.3. Chondrocyte adhesion, viability and proliferation

We next examined the interaction of the chondrocytes with the biomaterials. Live-dead assay demonstrated efficient cell attachment and evidence for cell proliferation (Fig. 6 and SEM analysis - Supplementary Fig. S2). The cells were also metabolically active (MTT assay - Supplementary Fig. S3). However, cells behaved differently on the scaffolds. On CHT scaffolds, cells tended to aggregate - as indicated, for example, by the green fluorescent spots on Fig. 6 (a–d). In contrast, cells tended to spread more evenly on scaffolds composed by CHT and PCL (Fig. 6 (e–h) and Supplementary Fig. S2 (e–h)) and 50CHT (Fig. 6 (i–l) and Supplementary Fig. S2 (i–l)). No differences were observed in metabolic activity (Supplementary Fig. S3 (e–h) and Supplementary Fig. S3 (i–l), respectively).

Water uptake ability is intrinsically related to the water affinity of the substrate. Surface tension can be affected by this factor, which is partially responsible and directly related to the degree of cell adhesion [36,37]. Surface energy (tension) of biomaterials may influence which serum proteins adhere to their surface, having a direct impact on their biological response, such as cell adhesion [38,39]. The widely accepted mechanism by which cells adhere to most TE scaffolds involves a two-step process: first, ECM proteins present in serum adsorb onto the scaffold material surface and, second, cells adhere to these scaffold-adsorbed proteins [40]. Both the composition and structure of this protein layer critically determines cell responses [41]. The homogeneous

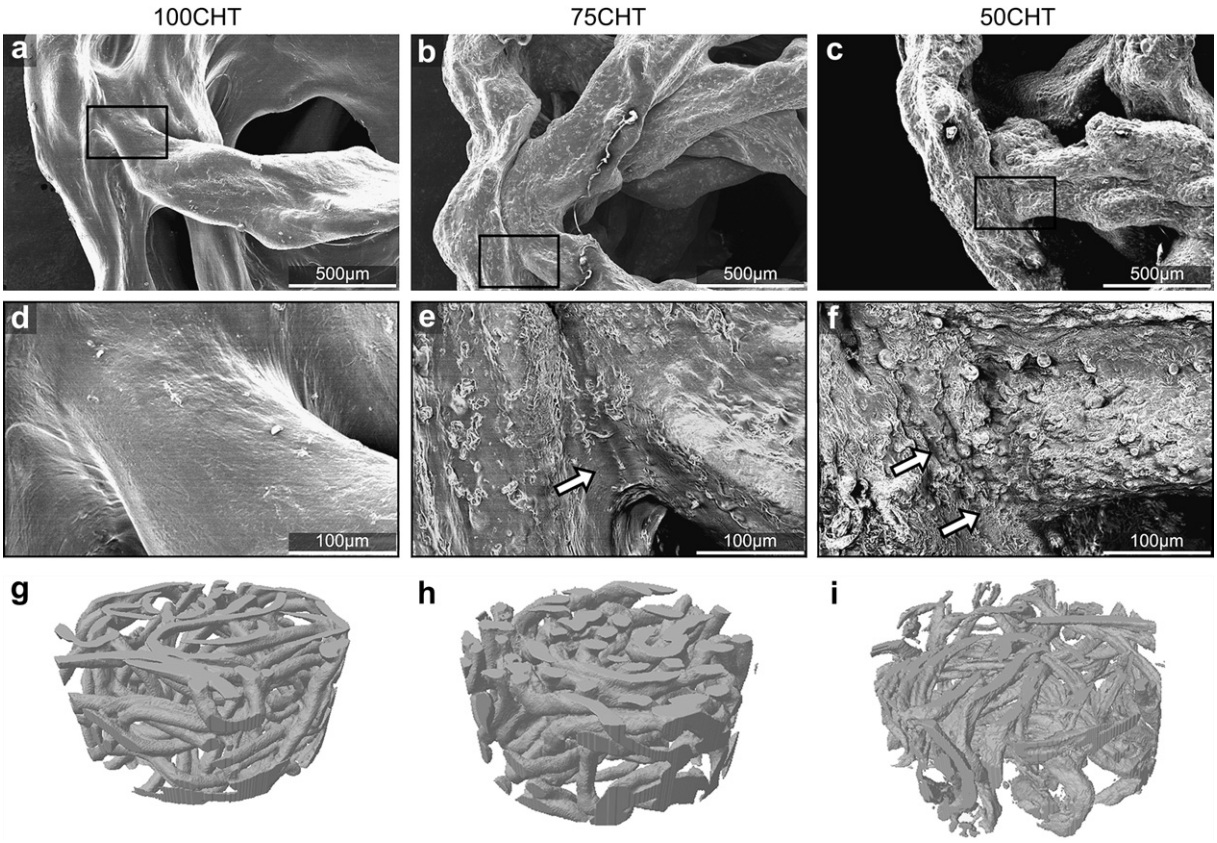

Fig. 5. SEM microphotographs of the (a, d) 100CHT, (b, e) 75CHT and (c, f) 50CHT fiber-meshes after the thermal treatment at $T_a = 60\ ^\circ C$ and $t_a = 3$ h. The (d–f) images correspond to the magnification of the area delimited by the rectangular box on the (a–c) images; representative 3D μCT images of the (g) 100CHT, (h) 75CHT and (i) 50CHT fiber-meshes.

surface dispersion of PCL and CHT is expected to balance the hydrophobic and hydrophilic features of both polymers.

Surface physical-chemical properties of biomaterials markedly influence cell adhesion as they have an impact on non-receptor mediated and receptor mediated attachment mechanisms [42]. Chondrocyte receptor mediated cell adhesion occurs via their attachment to many ECM proteins, such as fibronectin, vitronectin, various collagen types, perlecan and cartilage oligomeric matrix protein [43].

Chondrocyte-PCL interactions may be considered as non-receptor mediated cell adhesion, since PCL surfaces are considered inert for peptide conjugation [14,44]. Conversely, CHT presents similarities with some GAGs found on cartilaginous ECM. The combination of PCL and CHT domains in the blends may have been the main reason for the initial spreading of the chondrocytes, besides serum protein adhesion. Alternatively, cell distribution over the blends may also derive from the lack of binding sites over PCL domains and the chondrocytes consequent effort to find other cells or binding sites - like CHT domains. The proliferative behavioral shift observed, when comparing 100CHT with the blend fiber-meshes, is also related to the superficial hydrophilic/hydrophobic character of the fibers surface. Proteins present in proliferative medium may adhere differently to 100CHT and blend fibers due to a difference in surface energy. This may contribute to the difference in cell spreading. However, cell–material interactions are not only governed by the hydrophilic character of material surfaces or surface charge [45], even though moderately hydrophilic surfaces have been found to promote better cell adhesion [41]. Other surface properties such as roughness also influence cell behavior [31]. The differences on surface roughness between 100CHT and 75CHT/50CHT fiber-meshes may have also contributed to the dissimilar chondrocyte behavior observed.

Table 2
Mechanical properties of the scaffolds (standard deviation error also presented and (*) stands for statistical significant difference between formulations with $p < 0.05$) and their estimated and exemplificative porosity and pore size, obtained from the μCT analysis to the representative selected volumes presented on Fig. 5 (g–i).

Formulation	Young Modulus (kPa)	Porosity (%)	Pore Size (μm)
100CHT	4.43 (±0.29)*	75.6	330.2
75CHT	11.30 (±0.78)*	64.3	265.3
50CHT	23.63 (±3.36)*	83.2	384.7

3.4. Cartilaginous Ecm formation

The typical differentiated chondrogenic phenotype consists of chondrocytes that possess a rounded-like shape and that secrete ECM proteins, specifically collagen II and aggrecan, with a diffuse actin micro-filament network [46].

Chondrocytes morphology was monitored by analyzing the constructs using SEM during the differentiation studies (Fig. 7). The typical chondrogenic morphology was observed in all time-points for all fiber-mesh scaffolds formulations. In the differentiation studies, FBS derived protein adhesion onto the scaffolds cannot be responsible for cell adhesion to the fibers surfaces as the differentiation culture medium is serum-free. Therefore, direct cell–biomaterial interactions in combination with the influence of surface roughness is likely to play a role in cell attachment.

Histological evaluation (Fig. 8, Supplementary Fig. S4) showed that cartilaginous ECM production was present in all formulations at for both time-points analyzed (14 and 21 days). In all conditions examined, staining intensity increase with culture time is indicative

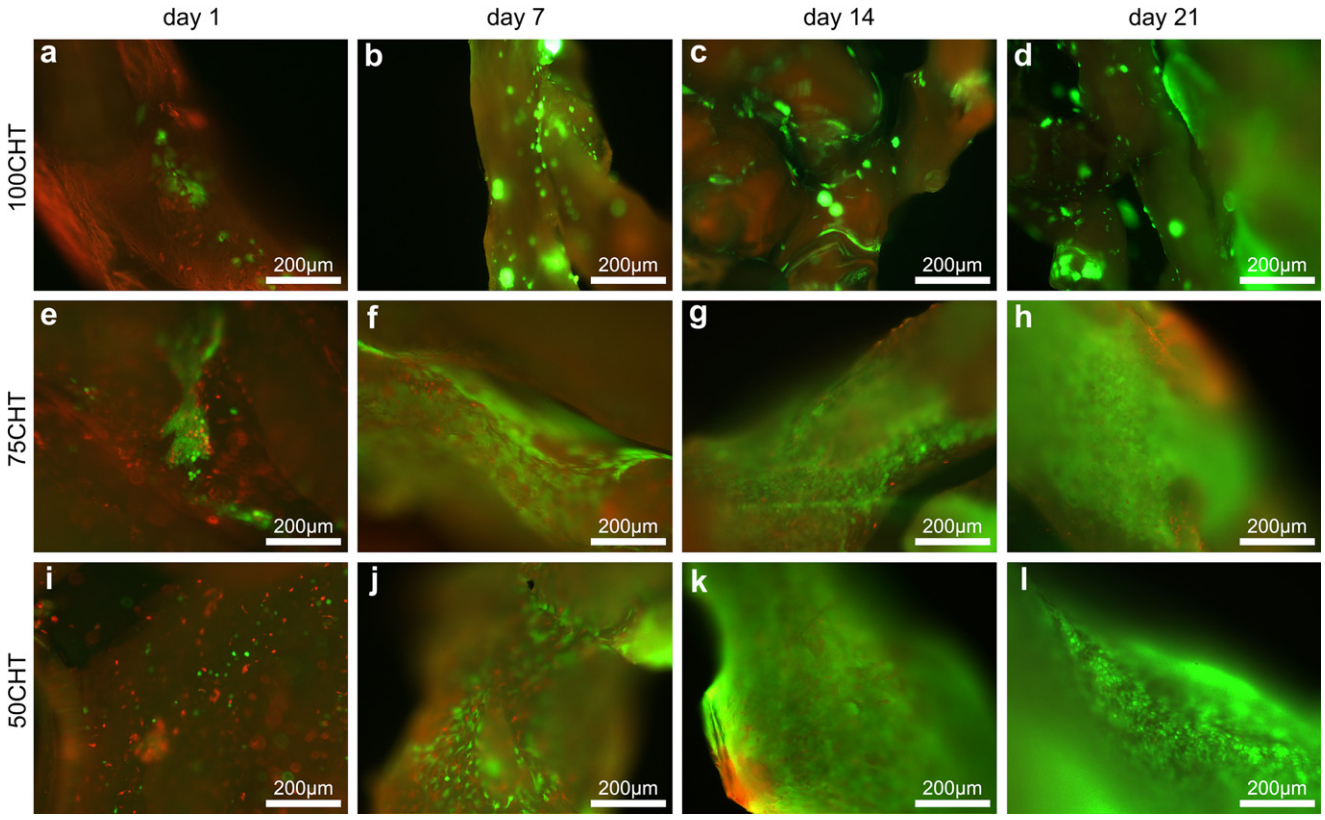

Fig. 6. Live-dead assay showing chondrocytes at scaffold fibers at day 1, 7, 14 and 21 of culture, in proliferation medium. Cells were stained with calcein-AM/ethidium homodimer (dead cells stain red and living cells green) and visualized using fluorescence microscopy. Cell density: 5×10^5 cells/20 μL.

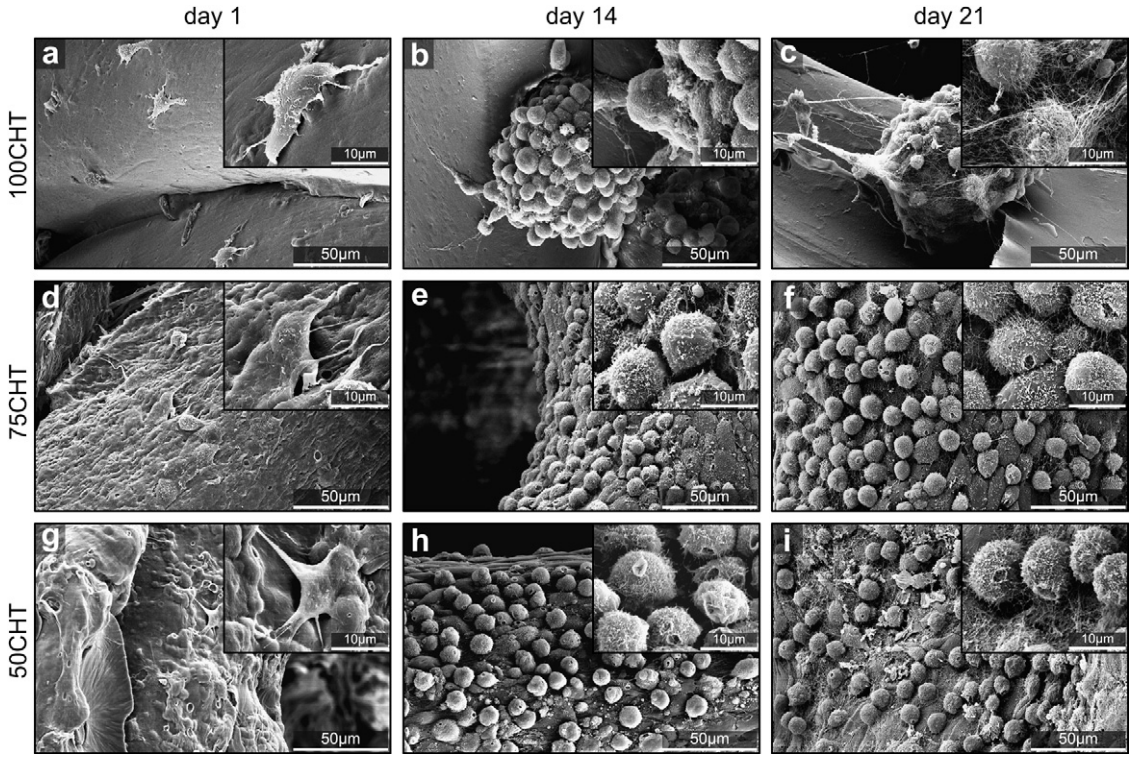

Fig. 7. SEM micrographs showing chondrocytes distribution and morphology over the scaffolds fibers surface after 1, 14 and 21 days in culture, with differentiation medium. Cell density: 5×10^5 cells/20 μL.

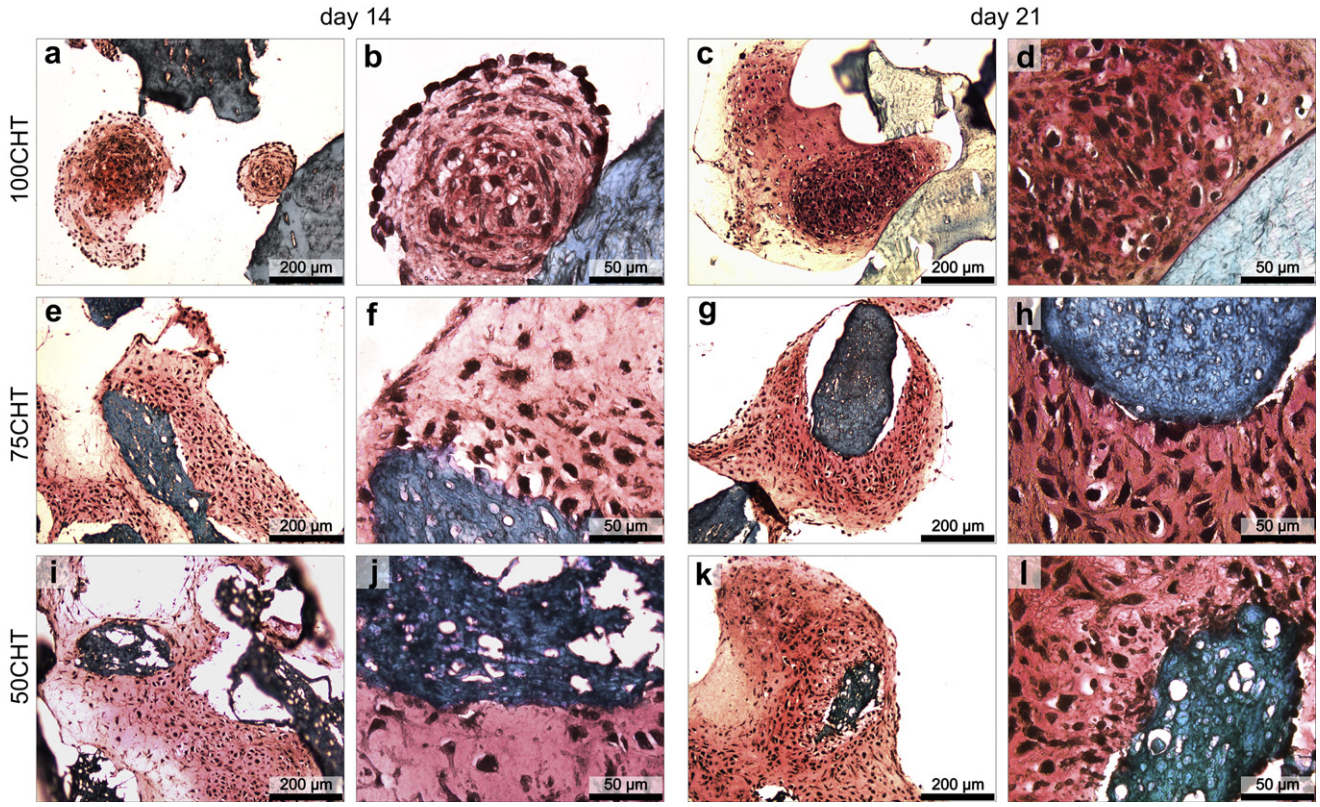

Fig. 8. Histological cross-sections show GAGs production (stained red) on the (a–d) 100CHT, (e–h) 75CHT and (i–l) 50CHT scaffolds, on day 14 (a, b, e, f, i, j) and day 21 (c, d, g, h, k, l) of culture in differentiation medium, by safranin-O staining. Cells are represented by the dark spots and bluish regions correspond to the scaffold material.

for ECM production. The histological analysis also reveals round-like cell aggregation in the 100CHT fiber-meshes (Fig. 8 (a–d) and Supplementary Fig. S4 (a–d)), in contrast to uniformly distributed round cells covering the scaffolds surface observed in the 75CHT and 50CHT formulations (Fig. 8 (e–l) and Supplementary Fig. S4 (e–l).

When chondrocytes maintain their natural spherical shape they produce more GAGs [47]. This fact is partly corroborated by the GAG/DNA ratio, i.e., GAG produced *per* cell. The DNA (Fig. 9(a)) and GAG (Fig. 9 (b) quantification assays, along with GAG/DNA ratio (Fig. 9 (c))), helped to better understand the chondrocytes activity within the scaffolds during the 21 days of culture.

At day 1, significant differences in cell amount (Fig. 9 (a)) were only observed between the 100CHT and the blend formulations. From day 1 to day 14, DNA amount increased for each scaffold formulation. On day 14, the DNA content was only significantly different between the 75CHT and the 100CHT and 50CHT formulations. From day 14 to day 21, the DNA amount significantly increased for 50CHT only, while this value remained unchanged for the other combinations.

GAG amount (Fig. 9 (b)) increased for all scaffold formulations over time. At day 1, GAG amount was not significantly different between formulations. From day 1 to day 14 (Fig. 9 (b)), there was a significant increase on GAG production by cells on all formulations.

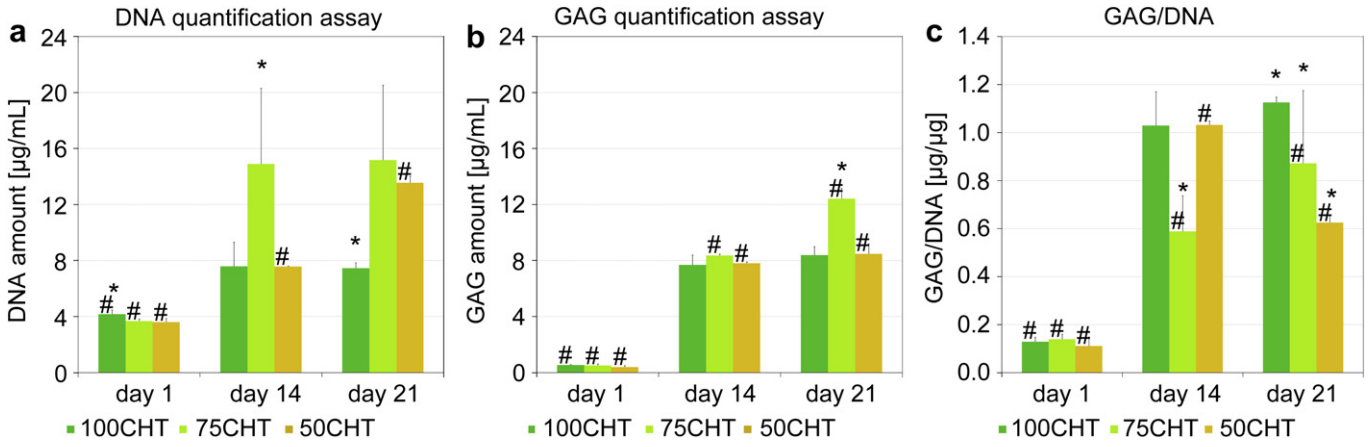

Fig. 9. (a) DNA and (b) GAG quantification assays and (c) GAG/DNA ratio of the constructs, after 1, 14 and 21 days of culture in differentiation medium. (*) stands for significant differences between different scaffold formulations on the same culture day ($p < 0.05$); (#) represents significant differences between the same scaffold formulation on different culture days ($p < 0.05$).

The highest production of GAG was observed for the 75CHT. From day 14 to day 21 (Fig. 9 (b)), all formulations had an increase in GAG amount. The highest production was again observed on 75CHT constructs, followed by the 100CHT and 50CHT constructs presenting a small increase.

The graphical representation of GAG/DNA ratios (Fig. 9 (c)) shows that, for the first day of culture, the ratios are similar between formulations. As expected, the GAG amount *per* cell amount was increased at the 14th day of culture. The highest ratio values corresponded to the 100CHT fiber and 50CHT constructs. With respect to day 21, 100CHT was the formulation with the highest GAG/DNA ratio, followed by the 75CHT constructs and, at last, the 50CHT.

Fig. 10 shows the over all distribution of ECM production over the scaffolds structure. On all fiber-meshes formulations, matrix quantity increased during the differentiation culture time period of 21 days. However, the distribution of the ECM throughout scaffolds was different depending on its composition. With respect to the 100CHT constructs, ECM distribution was confined to clusters at days 14 and 21 (Fig. 10 (b, c)), respectively. On the contrary, a homogeneous distribution of ECM was observed in the 75CHT (Fig. 10 (e, f)) and 50CHT (Fig. 10 (h, i)) fiber-meshes.

From the analysis of the SEM images present on Figs. 7 and 10, it can be observed that both 75CHT and 50CHT scaffolds resulted in a better distribution of the cells over the scaffold when compared to the 100CHT formulation. However, it is also known that cell aggregation enhances cell–cell signaling, resulting in a better tissue formation [48]. Cell distribution in the scaffold is an important parameter as it is related to ECM distribution as well. The scaffold design also implies that cells seeded may produce ECM to cover all the scaffold volume homogeneously. Thus, even if the GAG/DNA ratio was higher for the 100CHT constructs, it was observed that the ECM produced by chondrocytes over these constructs resulted into an undesired distribution. The poor spreading of the cells may also be related to the surface roughness, as commented before. Consequently, blend scaffolds would lead to a more homogeneous ECM production over the construct.

When comparing chondrocytes distribution over both blend scaffolds, there are no main differences. This indicates that both would lead to a homogeneous ECM dispersion over the scaffold. This effectively occurs, as proven by the over all observation of the constructs after the 21 days of differentiation culture (Fig. 10). The main difference was the chondrocytes behavior during the culturing days. On both blends, they proliferated until day 14, with significantly less cell number present on the 50CHT blend scaffolds. However, a major and important behavior shift occurred from day 14 to day 21, when comparing chondrocytes seeded in 75CHT and 50CHT scaffolds. For the 75CHT constructs, cells almost stopped proliferating and GAG production increased. On the contrary, for the 50CHT blend scaffolds, chondrocytes continued to proliferate and GAG production poorly increased. These results may indicate that chondrocytes seeded over the 50CHT tended to present fibroblast-like phenotypic de-differentiation. This leads to a proliferative behavior and a decrease in proteoglycan synthesis (along with a decreased type II collagen expression and increased type I collagen expression) [47]. The amount of CHT present in the 75CHT blend (i.e., the amount of domains similar to cartilaginous ECM) may also have helped chondrocytes to maintain their typical behavior.

The fiber's adhesion confers structural stability to the 3D constructs. The scaffolds maintained their structure after the compression tests and after cell proliferation and differentiation studies. Blending PCL with CHT improved the mechanical properties of CHT scaffolds, as evidenced by an increase in the Young

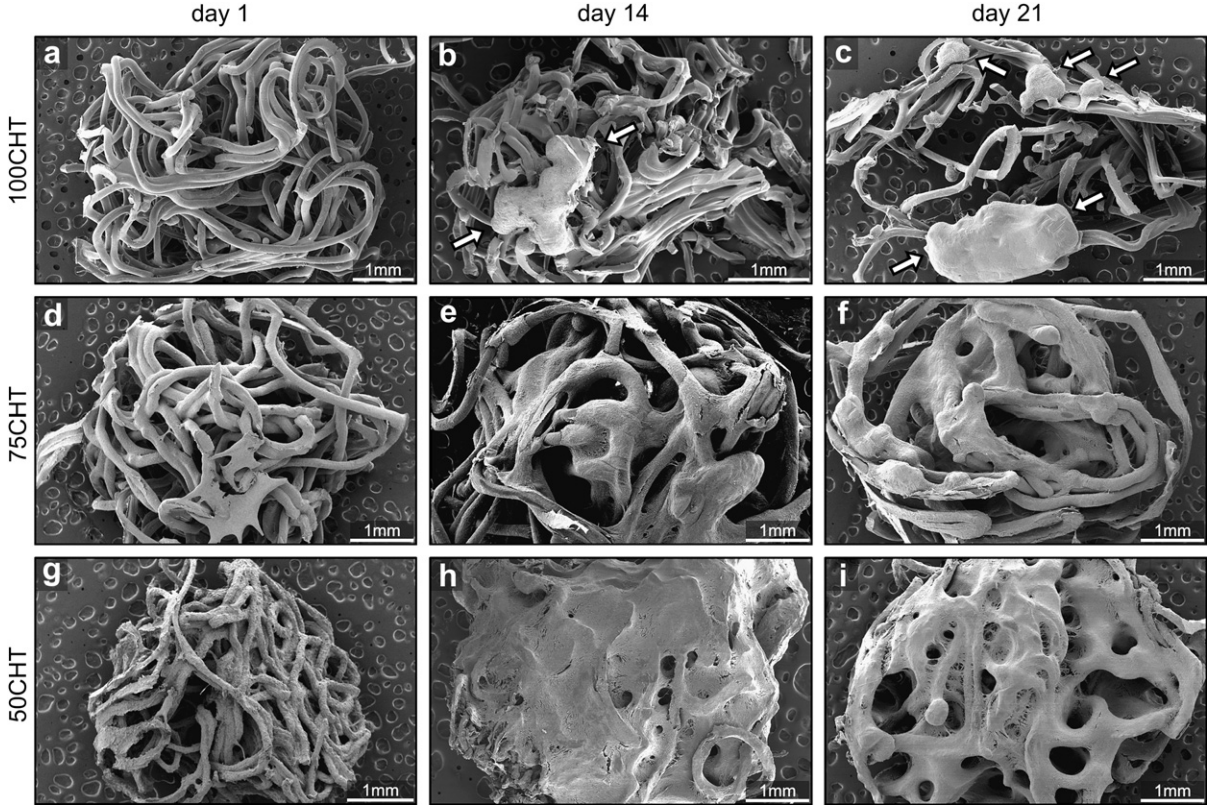

Fig. 10. SEM micrographs showing the 100CHT ECM distribution over the scaffolds after 1, 14 and 21 days in culture with differentiation medium. Arrows point out ECM aggregates.

modulus, with the highest values observed for the 50CHT scaffolds. However, the scaffolds mechanical properties did not exactly mimic those of AC. Besides the fact that AC has different zones, [2] which are not mimicked in the scaffold design, there are also main differences in the structural organization of cartilage and these fiber-mesh scaffolds. In normal cartilage developmental conditions *in vivo*, chondrocytes produce a very compact tissue and are embedded in a 3D matrix [2]. To facilitate cartilage formation *in vitro*, one needs to provide a 3D environment with ample possibilities for cell–cell contact and supply of nutrients. Our fiber-mesh scaffolds are primarily designed to match these needs. Consequently, the mechanical properties are not as good as those of AC, mainly due to their porosity and CHT content. It is believed, however, that during neo-cartilage formation the mechanical properties will improve. Particularly the homogeneous deposition of ECM in the CHT/PCL blends is likely to improve mechanical properties.

The 50CHT possesses a PCL amount that was proven to be too high (or a CHT quantity too low) that induced a loss of chondrogenic phenotype expression, despite the best mechanical performance. Even though the typical chondrocyte phenotype was maintained in 100CHT scaffolds, this formulation led to cell aggregation and consequently heterogeneous distribution of ECM. Therefore, we believe that the PCL quantity present on 75CHT altered CHT fibers properties in a balanced way, between the 50CHT and 100CHT formulations. Cell distribution over the 75CHT scaffolds was similar to that presented by the 50CHT, but the 75CHT structure was capable of maintaining chondrocytes phenotypical behavior in a similar way as the 100CHT. Despite the fact that 75CHT blend scaffolds showed a lower Young modulus, compared to the 50CHT scaffolds, it is (in long-term) expected that the 75CHT scaffold/neo-cartilage system would surpass the mechanical properties of the 50CHT scaffold/neo-cartilage system based on 75CHT biological performance.

4. Conclusions

100CHT, 75CHT and 50CHT fibers were successfully obtained by wet-spinning using a common solvent solution of 100 vol.% formic acid. The fibers were folded into cylindrical moulds and underwent a thermal treatment ($T_a = 60\ ^\circ C$; $t_a = 3$ h) to obtain the scaffolds. PCL domains were homogenously distributed over the blends, even if phase separation may exist at a micrometric scale. 3D fiber-mesh structures presented good integrity and stability, along with open and interconnected porosity and pore size range suitable for TE applications. PCL incorporation into CHT improved surface roughness of the fibers and diminished the swelling ratio. Blending improved cell spreading and did not affect cell survival nor did it impair metabolic activity. Regarding the differentiation studies, the 75CHT constructs performed the best, with the highest GAG amount and homogeneous ECM distribution. As the PCL content increased, the mechanical properties increased accordingly. However, as over 50CHT chondrocytes almost stopped producing GAG, the 75CHT formulation balanced at best the physical-chemical and biological properties of these new CHT/PCL blend 3D fiber-meshes for cartilage regeneration.

Acknowledgements

The research leading to these results has received funding from the European Union Seventh Framework Programme (FP7/2007-2013) under grant agreement number NMP4-SL-2009-229292 and it was also supported in part by a grant from the Dutch Program for Tissue Engineering (DPTE) to Liliana S. Moreira-Teixeira and Marcel Karperien.

Appendix. Supplementary data

Supplementary data associated with this article can be found in online version at doi:10.1016/j.biomaterials.2010.09.073.

Appendix

Figures with essential color discrimination. Figs. 2–4, 6, 8 and 9 in this article are difficult to interpret in black and white. The full color images can be found in the online version, at doi:10.1016/j.biomaterials.2010.09.073.

References

[1] Wakitani S, Kawaguchi A, Tokuhara Y, Takaoka K. Present status of and future direction for articular cartilage repair. J Bone Miner Metab 2008;26:115–22.
[2] Chung C, Burdick JA. Engineering cartilage tissue. Adv Drug Deliv Rev 2008;60:243–62.
[3] Kosher RA, Church RL. Stimulation of in vitro somite chondrogenesis by procollagen and collagen. Nature 1975;258:327–30.
[4] Suh JK, Matthew HW. Application of chitosan-based polysaccharide biomaterials in cartilage tissue engineering: a review. Biomaterials 2000;21:2589–98.
[5] Di Martino A, Sittinger M, Risbud MV. Chitosan: a versatile biopolymer for orthopaedic tissue-engineering. Biomaterials 2005;26:5983–90.
[6] Kuo YC, Lin CY. Effect of genipin-crosslinked chitin-chitosan scaffolds with hydroxyapatite modifications on the cultivation of bovine knee chondrocytes. Biotechnol Bioeng 2006;95:132–44.
[7] Kim SE, Park JH, Cho YW, Chung H, Jeong SY, Lee EB, et al. Porous chitosan scaffold containing microspheres loaded with transforming growth factor-β1: implications for cartilage tissue engineering. J Controlled Release 2003;91:365–74.
[8] Sarasam A, Madihally SV. Characterization of chitosan–polycaprolactone blends for tissue engineering applications. Biomaterials 2005;26:5500–8.
[9] Woodruff MA, Hutmacher DW. The return of a forgotten polymer - Polycaprolactone in the 21st century. Prog Polym Sci, in press. doi:10.1016/j.progpolymsci.2010.04.002, [Corrected Proof, Available online 7 April 2010].
[10] Ishaug-Riley SL, Okun LE, Prado G, Applegate MA, Ratcliffe A. Human articular chondrocyte adhesion and proliferation on synthetic biodegradable polymer films. Biomaterials 1999;20:2245–56.
[11] Hoque ME, San WY, Wei F, Li S, Huang M-H, Vert M, et al. Processing of polycaprolactone and polycaprolactone-based copolymers into 3D scaffolds, and their cellular responses. Tissue Eng A 2009;15:3013–24.
[12] Garcia-Giralt N, Izquierdo R, Nogués X, Perez-Olmedilla M, Benito P, Gómez-Ribelles JL, et al. A porous PCL scaffold promotes the human chondrocytes redifferentiation and hyaline-specific extracellular matrix protein synthesis. J Biomed Mater Res A 2008;85:1082–9.
[13] van Dijkhuizen-Radersma R, Moroni L, van Apeldoorn A, Zhang Z, Grijpma D. Degradable polymers for tissue engineering. Chapter 7. In: van Blitterswijk C, Thomsen P, Lindahl A, Hubbell J, Williams D, Cancedda R, de Bruijn J, Sohier J, editors. Tissue engineering. Academic Press Series in Biomedical Engineering; 2008. p. 202.
[14] Zhu Y, Gao C, Liu X, Shen J. Surface modification of polycaprolactone membrane via aminolysis and biomacromolecule immobilization for promoting cytocompatibility of human endothelial cells. Biomacromolecules 2002;3:1312–9.
[15] Cruz DMG, Coutinho DF, Martinez EC, Mano JF, Ribelles JLG, Sánchez MS. Blending polysaccharides with biodegradable polymers. II. Structure and biological response of chitosan/polycaprolactone blends. J Biomed Mater Res B 2008;87:544–54.
[16] Eyrich D, Wiese H, Maier G, Skodacek D, Appel B, Sarhan H, et al. In vitro and in vivo cartilage engineering using a combination of chondrocyte-seeded long-term stable fibrin gels and polycaprolactone-based polyurethane scaffolds. Tissue Eng 2007;13:2207–18.
[17] Malheiro VN, Caridade SG, Alves NM, Mano JF. New poly(ε-caprolactone)/chitosan blend fibers for tissue engineering applications. Acta Biomater 2010;6:418–28.
[18] Honma T, Senda T, Inoue Y. Thermal properties and crystallization behaviour of blends of poly(epsilon-caprolactone) with chitin and chitosan. Polym Int 2003;52:1839–46.
[19] Senda T, He Y, Inoue Y. Biodegradable blends of poly(epsilon-caprolactone) with alpha-chitin and chitosan: specific interactions, thermal properties and crystallization behavior. Polym Int 2002;51:33–9.
[20] Cruz DMG, Ribelles JLG, Sanchez MS. Blending polysaccharides with biodegradable polymers. I. Properties of chitosan/polycaprolactone blends. J Biomed Mater Res B 2008;85:303–13.
[21] Nielsen GD, Abraham MH, Hansen LF, Hammer M, Cooksey CJ, Andonian-Haftvan J, et al. Sensory irritation mechanisms investigated from model compounds: trifluoroethanol, hexafluoroisopropanol and methyl hexafluoroisopropyl ether. Arch Toxicol 1996;70:319–28.

[22] Sarasam AR, Samli AI, Hess L, Ihnat MA, Madihally SV. Blending chitosan with polycaprolactone: porous scaffolds and toxicity. Macromol Biosci 2007;7:1160–7.
[23] Wan Y, Wu H, Cao X, Dalai S. Compressive mechanical properties and biodegradability of porous poly(caprolactone)/chitosan scaffolds. Polym Degrad Stab 2008;93:1736–41.
[24] Wan Y, Xiao B, Dalai S, Cao X, Wu Q. Development of polycaprolactone/chitosan blend porous scaffolds. J Mater Sci Mater Med 2009;20:719–24.
[25] Wan Y, Cao X, Zhang S, Wang S, Wu Q. Fibrous poly(chitosan-g-DL-lactic acid) scaffolds prepared via electro-wet-spinning. Acta Biomater 2008;4:876–86.
[26] Tuzlakoglu K, Alves CM, Mano JF, Reis RL. Production and characterization of chitosan fibers and 3-D fiber mesh scaffolds for tissue engineering applications. Macromol Biosci 2004;4:811–9.
[27] Prabhakaran MP, Venugopal JR, Chyan TT, Hai LB, Chan CK, Lim AY, et al. Electrospun biocomposite nanofibrous scaffolds for neural tissue engineering. Tissue Eng A 2008;14:1787–97.
[28] Yang X, Chen X, Wang H. Acceleration of osteogenic differentiation of preosteoblastic cells by chitosan containing nanofibrous scaffolds. Biomacromolecules 2009;10:2772–8.
[29] Shalumon KT, Anulekha KH, Girish CM, Prasanth R, Nair SV, Jayakumar R. Single step electrospinning of chitosan/poly(caprolactone) nanofibers using formic acid/acetone solvent mixture. Carbohydr Polym 2010;80:413–9.
[30] Chiono V, Vozzi G, D'Acunto M, Brinzi S, Domenici C, Vozzi F, et al. Characterisation of blends between poly(ε-caprolactone) and polysaccharides for tissue engineering applications. Materi Sci Eng C 2009;29:2174–87.
[31] Lien SM, Ko LY, Huang TJ. Effect of pore size on ECM secretion and cell growth in gelatin scaffold for articular cartilage tissue engineering. Acta Biomater 2009;5:670–9.
[32] Alves da Silva ML, Crawford A, Mundy JM, Correlo VM, Sol P, Bhattacharya M. Chitosan/polyester-based scaffolds for cartilage tissue engineering: assessment of extracellular matrix formation. Acta Biomater 2010;6:1149–57.
[33] Olabarrieta I, Forsstrom D, Gedde UW, Hedenqvist MS. Transport properties of chitosan and whey blended with poly(ε-caprolactone) assessed by standard permeability measurements and microcalorimetry. Polymer 2001;42:4401–8.
[34] She H, Xiao X, Liu R. Preparation and characterization of polycaprolactone-chitosan composites for tissue engineering applications. J Mater Sci 2007;42:8113–9.
[35] Wan Y, Lu X, Dalai S, Zhang J. Thermophysical properties of polycaprolactone/chitosan blend membranes. Thermochim Acta 2009;487:33–8.
[36] Lampin M, Warocquier-Clérout Legris C, Degrange M, Sigot-Luizard MF. Correlation between substratum roughness and wettability, cell adhesion, and cell migration. J Biomed Mater Res 1998;36:99–108.
[37] Chang G, Absolom DR, Strong AB, Stubley GD, Zingg W. Physical and hydrodynamic factors affecting chondrocyte adhesion to polymer surfaces. J Biomed Mater Res 1988;22:13–29.
[38] Boyan BD, Hummert TW, Dean DD, Schwartz Z. Role of material surfaces in regulating bone and cartilage cell response. Biomaterials 1996;17:137–46.
[39] Olivieri MP, Rittle KH, Tweden KS, Loomis RE. Comparative biophysical study of adsorbed calf serum, fetal bovine serum and mussel adhesive protein. Biomaterials 1992;13:201–8.
[40] Liu H, Webster TJ. Nanomedicine for implants: a review of studies and necessary experimental tools. Biomaterials 2007;28:354–69.
[41] Elbert DL, Hubbell JA. Surface treatments of polymers for biocompatibility. Annu Rev Mater Sci 1996;26:365–94.
[42] Tsai WB, Wang MC. Effects of an avidin-biotin binding system on chondrocyte adhesion and growth on biodegradable polymers. Macromol Biosci 2005;5:214–21.
[43] Wyre RM, Downes S. The role of protein adsorption on chondrocyte adhesion to a heterocyclic methacrylate polymer system. Biomaterials 2002;23:357–64.
[44] Santiago LY, Nowak RW, Rubin JP, Marra KG. Peptide-surface modification of poly(caprolactone) with laminin-derived sequences for adipose-derived stem cell applications. Biomaterials 2006;27:2962–9.
[45] Lee JH, Khang G, Lee JW, Lee HB. Platelet adhesion onto chargeable functional group gradient surfaces. J Biomed Mater Res 1998;40:180–6.
[46] Wang L, Verbruggen G, Almqvist K, Elewaut D, Broddelez C, Veys E. Flow cytometric analysis of the human articular chondrocyte phenotype in vitro. Osteoarthritis Cartilage 2001;9:73–84.
[47] Moroni L, Schotel R, Hamann D, de Wijn JR, van Blitterswijk CA. 3D fiber-deposited electrospun integrated scaffolds enhance cartilage tissue formation. Adv Func Mater 2008;18:53–60.
[48] Wong M, Kireeva ML, Kolesnikova TV, Lau LF. Cyr61, product of a growth factor-inducible immediate-early gene, regulates chondrogenesis in mouse limb bud mesenchymal cells. Dev Biol 1997;192:492–508.